Supporting Information

Direct observation of a single nanoparticle-ubiquitin corona formation

Feng Ding[1,2,*], Slaven Radic[1], Ran Chen[1], Pengyu Chen[1], Nicholas K. Geitner[1], Jared M Brown[3] and Pu Chun Ke[1,*]

[1]Department of Physics and Astronomy, Clemson University, [2]Deapartment of Biochemistry and Biophysics, School of Medicine, University of North Carolina at Chapel Hill, [3]Department of Pharmacology and Toxicology, Brody School of Medicine, East Carolina University

Methods

Experimental characterisation of AgNP-ubiquitin corona.

Transmission electron microscopy imaging of AgNP-ubiquitin corona. Direct observation of formed AgNP-ubiquitin coronae was performed by transmission electron microscopy (Hitachi H7600). Specifically, AgNPs (10 nM) were incubated at room temperature in deionized water (18 MΩ-cm) at neutral pH with ubiquitin (5 μM) for 2 h, pipetted on a copper grid and negatively stained with phosphotungstic acid (optically less dense material) for 10 min prior to imaging. Similar procedures were performed for the protein-free control AgNPs (10 nM).

Hydrodynamic size and zeta potential measurements. Citrate-coated AgNPs (BioPure, nominal size: 10 nm) were purchased from NanoComposix and dispersed in Milli-Q water to form a stock suspension of 1 mg/mL (300 nM). Lyophilized ubiquitin (Boston Biochem, isolated from plant *Arabidopsis thaliana*) of 5 mg was dissolved in 500 mL Milli-Q water to obtain a final concentration of 1 mM. The hydrodynamic sizes of AgNPs (34.9 nM), ubiquitin (10 mM), and AgNP-ubiquitin (molar ratio: 1:100; incubation: 2 h) were measured with three repeats each at room temperature using a Zetasizer (Nano-S90, Malvern) (**Supplementary Fig. S1)**. In addition, the zeta potentials of AgNPs (4.97 nM), ubiquitin (5 mM), and AgNP-ubiquitin (molar ratio: 1:1000; incubation: 2h) were obtained at pH 6.5 using a Zetasizer (Nano, Malvern).

UV-vis absorbance measurement. To infer the binding of ubiquitins onto AgNPs we carried out an absorbance measurement using a UV-vis spectrophotometer (Cary 300 BIO, Varian). For this measurement the final AgNP concentration was 1.74 nM, while the final ubiquitin concentration was 50 mM. The mixture of AgNP-ubiquitin was incubated for 2 h prior to the measurement. An absorbance peak induced by the surface plasmon resonance of AgNPs upon excitation was observed at 393 nm, which was redshifted to 407 nm for the absorbance peak of the AgNP-ubiquitin mixture.

Circular dichroism spectroscopy. To determine changes in the secondary structures of ubiquitin upon nanoparticle-protein corona formation we performed a CD measurement using a JASCO J-810 spectropolarimeter. AgNPs and ubiquitins of a molar ratio of 1:1000 were incubated for 2 h and were diluted in quartz cuvettes to match the sensitivity of the instrument. CD spectra were acquired at room temperature over a wavelength range of 200-300 nm and averaged over five

scans taken at a speed of 50 nm/min. The backgrounds of the AgNP and ubiquitin controls were subtracted accordingly. The averages derived from the CONTINLL-4 and CONTINLL-7 methods were used to calculate percents of the secondary structures of the protein, based on the linear dependence between structural fractions and the spectra[1].

Computational modeling of AgNP-ubiquitin corona. We combined both atomistic and coarse-grained molecular dynamics simulation to characterize the structure and dynamics of protein corona, where atomistic simulations were used to identify the binding modes between an individual ubiquitin and an AgNP, and coarse-grained simulations were used to characterise the corona formation between multiple ubiquitins and an AgNP.

Discrete molecular dynamics simulation. Detailed descriptions for DMD algorithm can be found elsewhere[2,3]. Briefly, inter-atomic interactions in DMD were modeled by square-well potential functions. Neighboring interactions (such as bonds, bond angles, and dihedrals) were modeled by infinitely deep square-well potentials. During a simulation, an atom's velocity remained constant until a potential step was encountered, upon which time it changed instantaneously according to the conservations of energy, momentum, and angular momentum. Simulations proceeded as a series of such collisions, with a rapid sorting algorithm used at each step to determine the subsequent collision.

The difference between DMD and traditional molecular dynamics is in the form of the interaction potential functions. Approximating continuous potentials with step functions, DMD simulations were reduced to event (collision)-driven molecular dynamics. The improved sampling efficiency of DMD over traditional molecular dynamics originates mainly from the rapid processing of collision events and localized updates of collisions (only collided atoms are required to update at each collision)[4]. At an adequately small step size, the discrete step function approaches the continuous potential function and DMD simulations become equivalent to traditional molecular dynamics. DMD simulations have been widely used to study biomolecules[4], such as protein folding[5], molecular recognitions[6], and protein aggregation[7].

Atomistic DMD model. We used the united-atom representation for proteins and citric acids (citrates), where all heavy atoms and polar hydrogens were explicitly modeled. The bonded interactions included covalent bonds, bond angles, and dihedrals. We included van der Waals, solvation, environment-dependent hydrogen bonding interactions, and electrostatics in the non-bonded interactions. The solvation energy was modeled using the Lazaridis-Karplus implicit solvation model with the fully-solvated conformation as the reference stated[8]. The hydrogen bond interaction was modeled using a reaction-like algorithm[9]. In addition to the previous version of the atomistic DMD force field[5], we also added electrostatic interactions between charges, including the basic and acidic residues in proteins[7] and charged groups in small molecules. The interaction parameters for citric acids were adapted from the Medusa force field extension for small molecules.[10] We used the Debye-Hückel approximation to model the screened charge-charge interactions. The Debye length was set at approximately 10 Å by assuming water relative permittivity of 80, and a monovalent electrolyte concentration of 0.1 mM. We used an interaction range of 30 Å for the electrostatic interactions, where the screened potential approached zero.

AgNP model. Because our knowledge of the interactions between nanoparticles and proteins is still lacking, there are no well-accepted force fields that can readily capture the binding between AgNP and proteins. In order to model the formation of AgNP-ubiquitin corona, we developed a simple model for simulating AgNP, where the model parameters were assigned to capture the general properties of the molecular system. Since the interactions between AgNP and proteins take place primarily on the surface of AgNP, we only explicitly modeled the surface atoms. The VDW radius of a silver atom is r=1.72 Å. Assuming close packing of silver atoms on the surface, we can calculate that the number of surface atoms for an AgNP with the diameter D=100 Å is $N=\pi D^2\rho_{2d}/\pi r^2$, where ρ_{2d} is the close packing density of ~0.84. Therefore, the total number of silver atoms is ~2,830 in one AgNP. We grouped every three atoms into one coarse-grained silver atom with a VDW radius of ~2.98 Å, and the number of surface atoms was reduced to 943. We introduced one atom in the center of the AgNP, and imposed distance constraints between the center and surface atoms at [49.5 Å, 50.5 Å]. As a result, all surface atoms effectively remained on the AgNP surface during simulations.

The same coarse-grained AgNP model was used in both all-atom and coarse-grained DMD simulations. In the all-atom simulations, the non-bonded interactions for AgNP surface atoms included van der Waals, solvation, and electrostatics. The VDW interaction between two atoms (*i* and *j*) in Medusa is proportional to $(\varepsilon_i\varepsilon_j)^{0.5}$, where $\varepsilon_i^{0.5}$ is the dipole polarisability of atom *i*. We assigned ε=0.4 for the coarse-grained surface atoms (comparing to ε=0.12 for carbonyl carbon in CHARMM 19[11]). For the Lazaridis-Karplus solvation interaction[8], we assumed a coarse-grained surface atom is hydrophobic and the free energy ΔG for excluding it from water is -2 kcal/mol.

AgNP is usually synthesized by chemical reduction of Ag+ salt and capped by the negatively charged citric acid, or citrate[12]. Due to incomplete reduction, it is likely that there are residual silver ions on the AgNP surface that bind to citrates. The citrate-capped AgNP alone had the zeta-potential of -45.0 mV, suggesting excessive citrate molecules. We randomly selected a subset of the surface atoms and assigned positive charges. We initially assigned +e to the charged surface atoms and performed equilibration simulations with excessive citrates. We found that citrate molecules with -3e had the tendency to attract multiple charged surface atoms (~3) to its vicinity, forming charged clusters (**Supplementary Fig. S5**). Since the charge-charge interactions are long-ranged and their calculations in DMD are proportional to the square of total number of charged atoms, we decided to assign a positive charge of +3e to the charged surface atoms in order to increase DMD sampling efficiency by reducing excessive calculations.

In the all-atom DMD simulations, the units of mass, length, and energy are Dalton (1.66×10^{-24} gram), angstrom (10^{-10} meter), and kcal/mol (6.9×10^{-22} joule), respectively. Given the units of mass [M], length [L], and energy [E], the time unit (t.u.) can be determined as approximately 50 femtoseconds.

Calculation of contacts between AgNP and ubiquitin. We defined a contact occurred between an ubiquitin residue and the AgNP when the distance between the AgNP center and the corresponding C_β atom of the residue was less than 57.5 Å. The protein was assumed to be AgNP-bound if at least one residue was in contact with the AgNP, and the contact frequency

between each residue and the AgNP was averaged over the total time that the protein remained bound to the AgNP.

Calculation of 2D-PMF. We first computed the 2D-histogram with respect to the center-of-mass distance between AgNP and ubiquitin, d_{cm}, and the number of contacts between AgNP and the subset of residues identified to bind specifically to AgNP, N_c. The inter-molecule distance d_{cm} was sampled from 60 Å to 120 Å with the bin size of 2.5 Å, while the sampling of N_c was from 0 to 13 with the bin size of 1. The 2D-PMF was simply computed proportional to the logarithm of population, $-K_bT\ln(P)$. Here, K_b is the Boltzmann constant and P is the population.

Coarse-grained molecular system. We used a two-bead-per-residue protein model for the study of corona formation between multiple ubiquitins and an AgNP[13,14]. In the two-bead model, each amino acid was represented by only the α-carbon (backbone) and β-carbon (sidechain). The bonded interactions between neighboring atoms along the peptide chain were assigned to mimic peptide geometry[14]. We used a structure-based potential to model the sidechain-sidechain packing interactions, where native interactions observed in the native state were favored. Two interacting residues can form either intra- or inter-monomer contacts, in order to promote protein-protein association[13,15]. The attractions between the residue β-carbons were assigned with a hard-core distance of D_{hc}=3 Å and an interaction range of D_{IR}=7.5 Å. The interaction strength of the native contact was ε, which was set as 1 kcal/mol. We also modeled the backbone-backbone hydrogen bond interaction as in Ref. [13], where each Cα can maximally form two hydrogen bonds with other Cα atoms, and two hydrogen bonds formed by one Cα atom are aligned co-linear[13] in order to model the angular dependence of hydrogen bonds. Other inter-atomic interaction for proteins was simply hard sphere collisions with the hardcore distant of D_{hc}=3 Å.

We determined the folding thermodynamics of an isolated coarse-grained ubiquitin by replica exchange DMD simulations[7]. Using weighted histogram analysis method[16,17], we calculated the specific heat and RMSD of ubiquitin as the function of simulation temperature (**Supplementary Fig. S2**). The specific heat featured a single peak at T_f = 340K, which corresponded to the melting temperature of the protein. Below T_f the protein remained folded with low RMSD, which was comparable to all-atom simulations (Fig. 3b). Above T_f, the protein became unfolded with large RMSD.

Each citric acid was represented by one coarse-grained atom. We used the same AgNP model as described above and assigned a strong attraction between citrates and the charged AgNP surface atoms. The citrates showed a weak repulsion to ubiquitin to mimic the mutually exclusive binding to AgNP as observed in atomistic simulations. We assigned a more favorable attraction between the charged AgNP atoms and the AgNP-binding residues (residues 18, 19, 20, 21, 22, 24, 25, 28, 52, 54, 55, 57, and 58), compared to the rest of the protein. The interaction parameters are summarized in the **Supplementary Table S1**.

Simulation setups and conditions.

i) *Atomistic simulations*. The molecular system was composed of one AgNP, one ubiquitin, and 50 citrates (-3e). The molecules were placed in a 150 x 150 x 150 $Å^3$ cubic box with periodic boundary conditions. We set a subset of 40 surface atoms of AgNP (randomly distributed) as

positively charged (3e), and kept the center atom fixed during the simulations. The excessive citrates were included to capture the experimentally observed negative zeta-potential of citrate-capped AgNP. The simulation temperature was maintained at 300 K using an Anderson thermostat[18]. The molecular system of the AgNP and citrates was equilibrated at first in order to let citrates bind to the surface charges (**Supplementary Fig. S6**). In the control simulations of artificially enhanced electrostatic interactions between citrates and the AgNP, we added an additional charge (-e) to the C6 atom of the citrate molecule (**Supplementary Fig. S7**)

ii) *Coarse-grained simulations.* There were one AgNP, 25 (or 50) ubiquitins, and 80 citrates in a 300 x 300 x 300 $Å^3$ cubic box with periodic boundary conditions. A subset of 60 AgNP surface atoms was positively charged, and the AgNP center was also kept static. We performed the simulations at a constant temperature of 325 K, which was set to enhance the kinetics while still below the melting point (**Supplementary Fig. S2)**.

Fitting analysis of the AgNP-ubiquitin binding kinetics.
We used the least square (χ^2) approach to fit the ubiquitin-AgNP binding data derived from coarse-grained DMD simulations. Since the data was approximately linear in the log-log plot (**Fig. 4** & **Supplementary Fig. S8**), we fitted the data with three different models, including a power-law, $\sim t^{\alpha}$, a stretched exponential, $\sim 1-exp(-ct^{\alpha})$, and a cumulative lognormal, $\sim 1+erf(c\ln(t/\tau))$. Here, *erf* is the error function. Among three fitting models, the power-law gave the largest χ^2-value, 962.4. The fitting for both the stretched exponential and cumulative lognormal functions were similar, with χ^2-values equal to 469.1 and 486.8, respectively. A lognormal distribution is usually used to describe the data where the value is the multiplicative product of many independent random variables. The relaxation time cannot be modeled as the product of a large number of independent random variables. On the other hand, a stretched exponential function is often used to describe the relaxation kinetics with high heterogeneity in relaxation time, where the kinetics can be described as linear superposition of exponential decays with continuous distribution of relaxation time. A similar stretched exponential binding kinetics has been observed in a fluorescence study of protein binding to colloidal nanoparticles[19]. Therefore, the stretched exponential (α=0.34) better characterized the ubiquitin-AgNP binding kinetics.

References

[1] Chen, R.; Choudhary, P.; Schurr, R. N.; Bhattacharya, P.; Brown, J. M.; Chun Ke, P. *Appl Phys Lett* **2012**, *100*, 13703-13707.
[2] Allen, M. P., and Tildersley, D.J. *Computer simulation of liquids*; Clarendon Press: New York, NY, USA, 1989.
[3] Rapapport, D. C. *The art of molecular dynamics simulation*; Cambridge University Press: Cambridge, 1997.
[4] Ding, F.; Dokholyan, N. V. In *Computational Modeling of Biological Systems: From Molecules to Pathways*; Dokholyan, N. V., Ed.; Springer: 2012, p 57-73.
[5] Ding, F.; Tsao, D.; Nie, H.; Dokholyan, N. V. *Structure* **2008**, *16*, 1010-8.

[6] Dagliyan, O.; Proctor, E. A.; D'Auria, K. M.; Ding, F.; Dokholyan, N. V. *Structure* **2011**, *19*, 1837-45.
[7] Ding, F.; Furukawa, Y.; Nukina, N.; Dokholyan, N. V. *J Mol Biol* **2012**, *421*, 548-60.
[8] Lazaridis, T.; Karplus, M. *Curr Opin Struct Biol* **2000**, *10*, 139-45.
[9] Ding, F.; Borreguero, J. M.; Buldyrey, S. V.; Stanley, H. E.; Dokholyan, N. V. *Proteins* **2003**, *53*, 220-8.
[10] Yin, S.; Biedermannova, L.; Vondrasek, J.; Dokholyan, N. V. *J Chem Inf Model* **2008**, *48*, 1656-62.
[11] Neria, E.; Fischer, S.; Karplus, M. *Journal of Chemical Physics* **1996**, *105*, 1902-1921.
[12] Henglein, A.; Giersig, M. *Journal of Physical Chemistry B* **1999**, *103*, 9533-9539.
[13] Ding, F.; Dokholyan, N. V.; Buldyrev, S. V.; Stanley, H. E.; Shakhnovich, E. I. *J Mol Biol* **2002**, *324*, 851-7.
[14] Ding, F.; Dokholyan, N. V.; Buldyrev, S. V.; Stanley, H. E.; Shakhnovich, E. I. *Biophys J* **2002**, *83*, 3525-32.
[15] Yang, S.; Cho, S. S.; Levy, Y.; Cheung, M. S.; Levine, H.; Wolynes, P. G.; Onuchic, J. N. *Proc Natl Acad Sci U S A* **2004**, *101*, 13786-91.
[16] Kumar, S.; Bouzida, D.; Swendsen, R. H.; Kollman, P. A.; Rosenberg, J. M. *Journal of Computational Chemistry* **1992**, *13*, 1011-1021.
[17] Chodera, J. D.; Swope, W. C.; Pitera, J. W.; Seok, C.; Dill, K. A. *Journal of Chemical Theory and Computation* **2007**, *3*, 26-41.
[18] Andersen, H. C. *J Chem Phys* **1980**, *72*, 2384-2393.
[19] Rocker, C.; Potzl, M.; Zhang, F.; Parak, W. J.; Nienhaus, G. U. *Nat Nanotechnol* **2009**, *4*, 577-80.

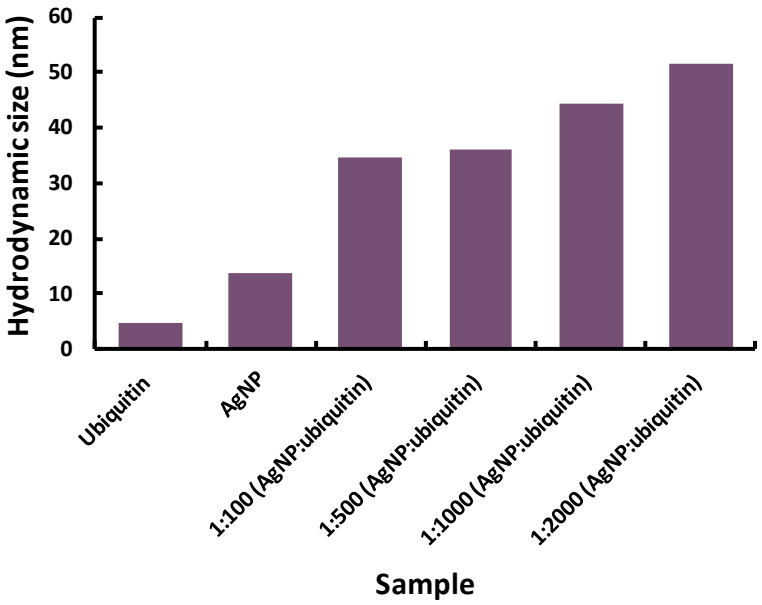

Figure S1. Hydrodynamic size of AgNP-ubiquitin corona at different molar ratios.

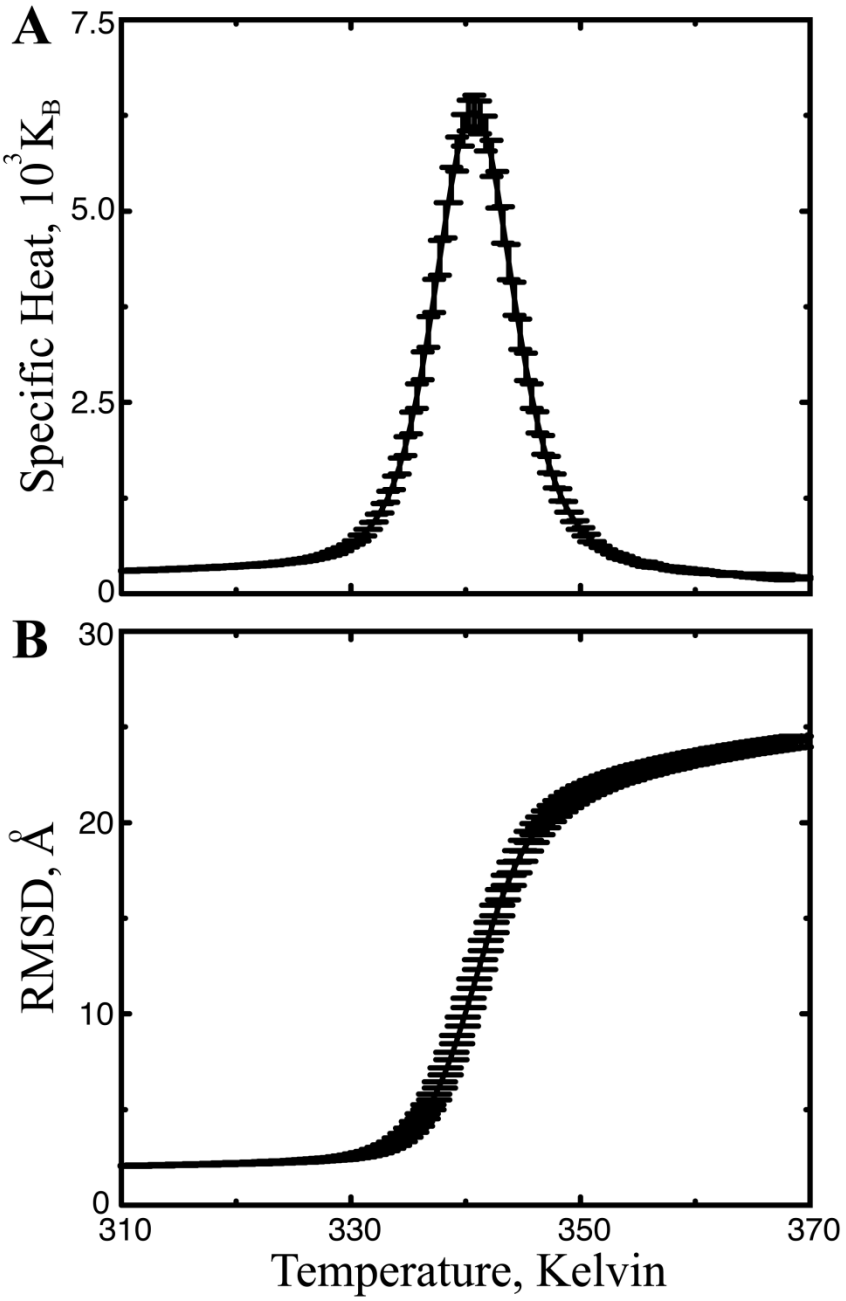

Figure S2. The folding thermodynamics of the coarse-grained ubiquitin. The specific heat (A) and RMSD (B) were computed as the function of the simulation temperature using replica exchange simulations and weighted histogram analysis. The error bars were computed as the statistical uncertainty[17].

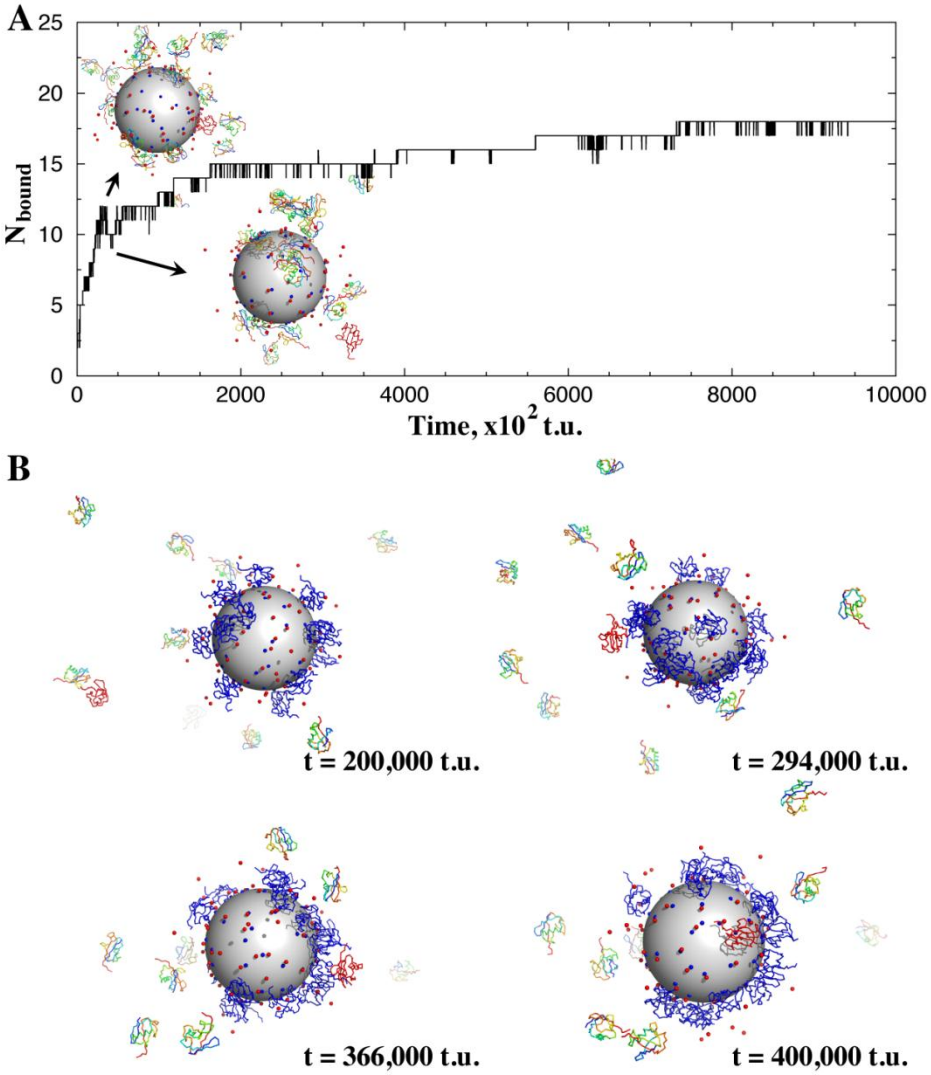

Figure S3. The kinetics of ubiquitin-AgNP binding. (a) The number of ubiquitin molecules bound to AgNP, N_{bound}, as the function of time (in DMD time unit, t.u., see Supporting Information) from a typical DMD simulation. The backbone trace of ubiquitin (rainbow color) is shown. The citrates correspond to the red spheres. The large gray sphere denotes the AgNP, and the blue spheres on the surface of the AgNP are the positively charged atoms. The insert illustrates the association and dissociation of a ubiquitin (in red). (b) The snapshots along the DMD simulation trajectory demonstrate the non-specific binding between incoming ubiquitin and proteins already bound to AgNP, which slows down the association.

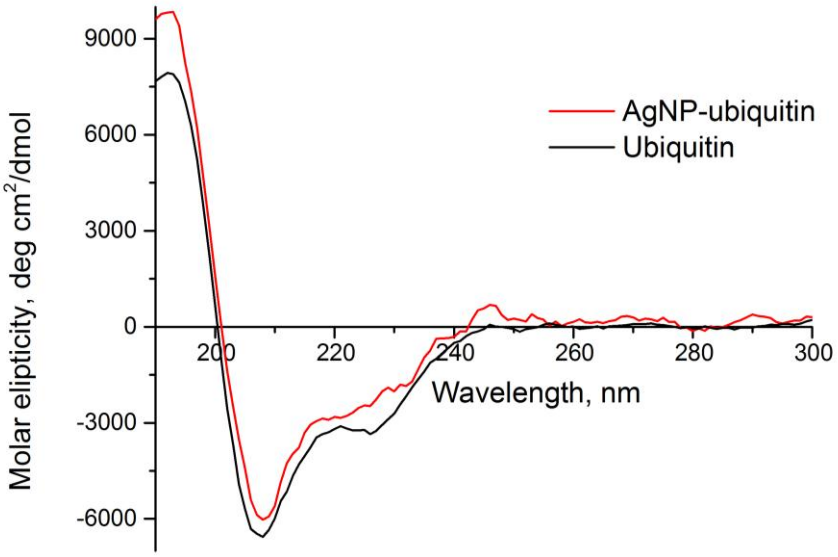

Figure S4. The CD spectra of both ubiquitin (black) and AgNP-ubiquitin (red).

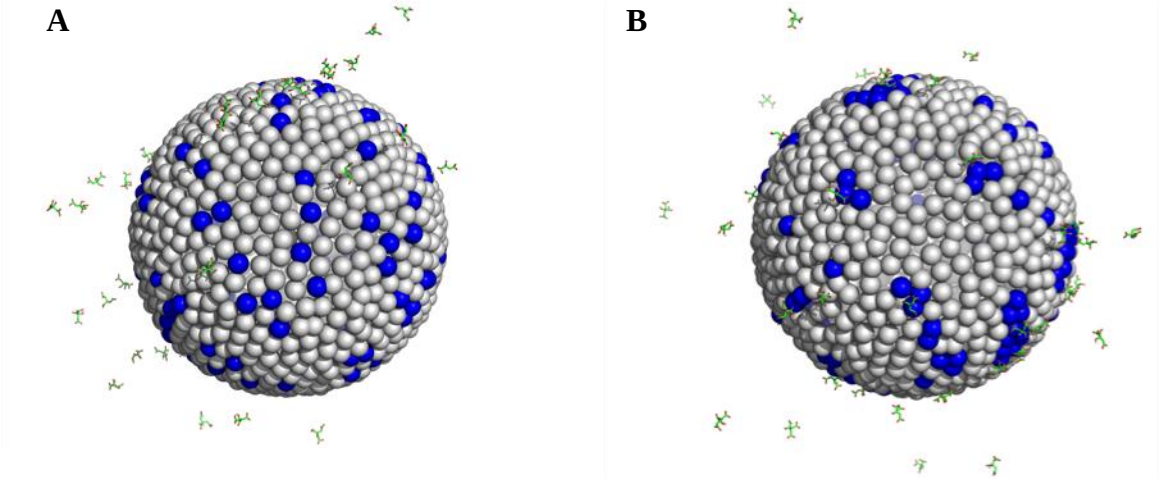

Figure S5. The equilibration of citrates and AgNP. The coarse-grained surface atoms are shown as spheres, where the charged atoms are colored blue and uncharged atoms are gray. The citrate is shown in stick representation. (A) Initially, the charges (+e) were randomly distributed on the surface and citrates were not bound. (B) During the equilibration simulations, the citrates with -3e had the tendency to attract multiple charged atoms (~3) together.

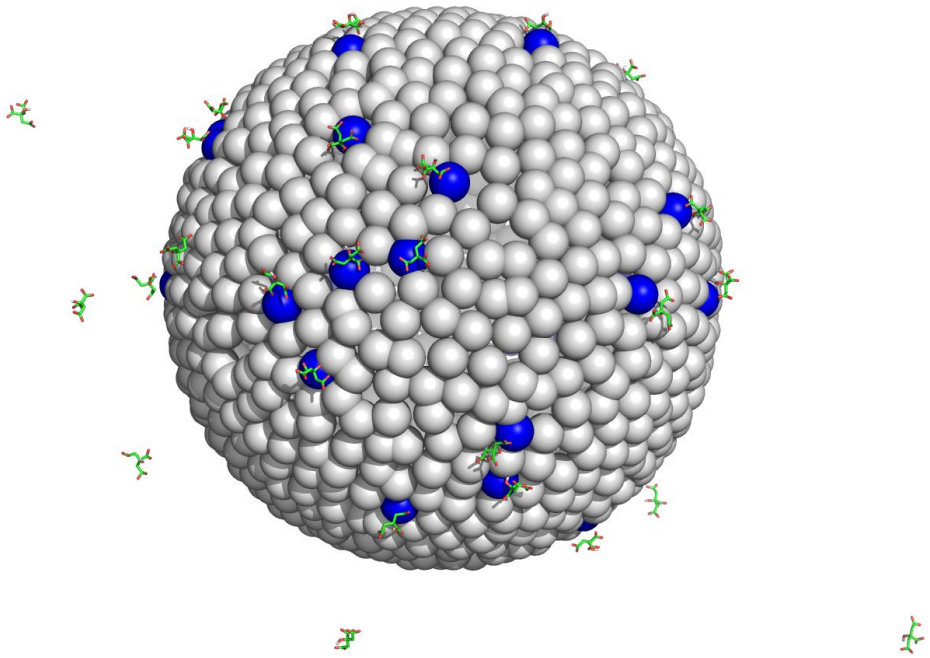

Figure S6. The equilibrated state of citrate-capped AgNP. The charged surface atoms (+3e) are shown as blue spheres, and the rest surface AgNP atoms are represented as gray spheres. The negatively-charged citrates (-3e) bind to the charged AgNP surface atoms, while there are excessive citrates in the solution.

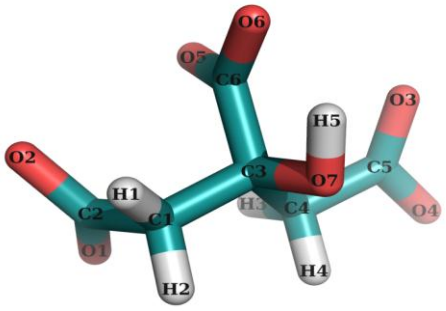

Figure S7. The molecular structure of citrate. The citrate molecule is in stick representation and the atoms are specifically labeled.

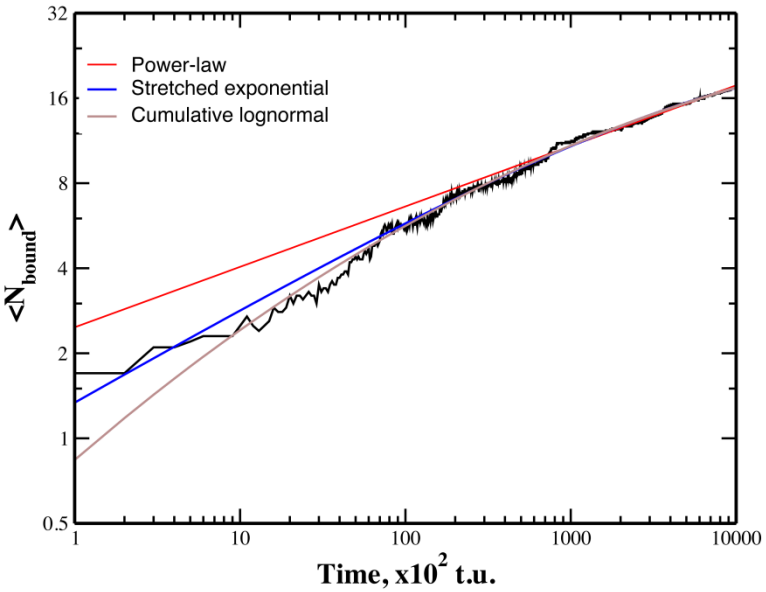

Figure S8. The ubiquitin-AgNP binding kinetics. The average number of ubiquitins bound to AgNP, $<N_{bound}>$, was computed as the function of simulation time in a log-log plot (black line). Using the least square method, the data was fitted with a power-law (red line), a stretched exponential (blue), and a cumulative lognormal (brown).

Table S1. Interaction parameters between coarse-grained atoms. Most of the interactions were modeled by a single-well DMD potential, where D_{hc} denoted the hard-core distance, D_{IR} indicated the interaction range beyond which two atoms did not interact, and E_{rep} and E_{attr} corresponded to the repulsive (>0) and attractive (<0) energy steps, correspondingly. The energy unit, ε, was set as 1 kcal/mol. A hard sphere collision potential between atoms was defined by the hard-core distance, D_{hc}. The charged AgNP surface atoms interacted with each other via the screened electrostatic repulsion as described in the all-atom simulations (Methods). The AgNP-binding involved residues 18, 19, 20, 21, 22, 24, 25, 28, 52, 54, 55, 57, and 58, which featured high contact frequencies as revealed by the all-atom simulations. The interactions between inter- and intra-protein atom pairs were modeled by the structure-based potentials[13,15].

<table>
<tr><td rowspan="2"></td><td rowspan="2">Citrate</td><td colspan="2">AgNP atom</td><td colspan="3">Ubiquitin</td></tr>
<tr><td>Uncharged</td><td>Charged</td><td>AgNP-binding residue, C_β</td><td>Other residue, C_β</td><td>Backbone Cα</td></tr>
<tr><td>Citrate</td><td>D_{hc} = 4.5Å
D_{IR} = 7.5Å
E_{rep} = 2ε</td><td>D_{hc} = 4.5Å
D_{IR} = 7.5Å
E_{rep} = -1.2ε</td><td>D_{hc} = 4.5Å
D_{IR} = 7.5Å
E_{attr}= -4.2ε</td><td colspan="2">D_{hc} = 4.5Å
D_{IR} = 7.5Å
E_{rep} = 0.4ε</td><td rowspan="3">Hard sphere:
D_{hc} = 4.5 Å</td></tr>
<tr><td>Uncharged AgNP atoms</td><td>D_{hc} = 4.5 Å
D_{IR} = 7.5Å
E_{rep} = -1.2ε</td><td>Hard sphere:
D_{hc} = 5.95 Å</td><td>Hard sphere:
D_{hc} = 5.95 Å</td><td colspan="2">D_{hc} = 4.5 Å
D_{IR} = 7.5Å
E_{attr}= -0.4ε</td></tr>
<tr><td>Charged AgNP atoms</td><td>D_{hc} = 4.5 Å
D_{IR} = 7.5Å
E_{attr}= -4.2ε</td><td>Hard sphere:
D_{hc} = 5.95 Å</td><td>Electrostatic repulsion</td><td>D_{hc} = 4.5 Å
D_{IR} = 7.5Å
E_{attr}= -1.0ε</td><td>D_{hc} = 4.5 Å
D_{IR} = 7.5Å
E_{attr}= -0.4ε</td></tr>
<tr><td>AgNP-binding residue, C_β</td><td rowspan="2">D_{hc} = 4.5 Å
D_{IR} = 7.5Å
E_{rep} = 0.4ε</td><td rowspan="2">D_{hc} = 4.5 Å
D_{IR} = 7.5Å
E_{attr}= -0.4ε</td><td>D_{hc} = 4.5 Å
D_{IR} = 7.5Å
E_{attr}= -1.0ε</td><td colspan="3" rowspan="2">Structure-based interaction potential (Methods)</td></tr>
<tr><td>Other residue, C_β</td><td>D_{hc} = 4.5 Å
D_{IR} = 7.5Å
E_{attr}= -0.4ε</td></tr>
<tr><td>Backbone Cα</td><td colspan="3">Hard sphere: D_{hc} = 4.5 Å</td><td colspan="3"></td></tr>
</table>